

**Reaction and fusion cross sections for the near-symmetric system  $^{129}\text{Xe} + ^{\text{nat}}\text{Sn}$  from 8A to 35A MeV**

L. Manduci,<sup>1,2</sup> O. Lopez,<sup>2</sup> A. Chbihi,<sup>3</sup> M. F. Rivet,<sup>4,\*</sup> R. Bougault,<sup>2</sup> J. D. Frankland,<sup>3</sup> B. Borderie,<sup>4</sup> E. Galichet,<sup>4,5</sup> M. La Commara,<sup>6</sup> N. Le Neindre,<sup>2</sup> I. Lombardo,<sup>6</sup> M. Pârlog,<sup>2</sup> E. Rosato,<sup>6,\*</sup> R. Roy,<sup>7</sup> G. Verde,<sup>4,8</sup> and E. Vient<sup>2</sup>  
(INDRA Collaboration)

<sup>1</sup>*Ecole des Applications Militaires de l'Energie Atomique, Postal Box BP 19 50115, Cherbourg Armées, France*

<sup>2</sup>*Laboratoire de Physique Corpusculaire, ENSICAEN, Université de Caen, CNRS/IN2P3, F-14050 Caen Cedex, France*

<sup>3</sup>*Grand Accélérateur National d'Ions Lourds, CEA and CNRS/IN2P3, Postal Box BP 5027, F-14076 Caen Cedex, France*

<sup>4</sup>*Institut de Physique Nucléaire, CNRS/IN2P3, Université Paris-Sud 11, F-91406 Orsay Cedex, France*

<sup>5</sup>*Conservatoire National des Arts et Métiers, F-75141 Paris Cedex 03, France*

<sup>6</sup>*Dipartimento di Scienze Fisiche and Sezione INFN, Università di Napoli "Federico II", I-80126 Napoli, Italy*

<sup>7</sup>*Laboratoire de Physique Nucléaire, Université Laval, Québec G1K 7P4, Canada*

<sup>8</sup>*INFN-Sezione Catania, via Santa Sofia, 64, 95123 Catania, Italy*

(Received 11 July 2016; published 18 October 2016)

**Background:** We study heavy-ion reactions from barrier up to Fermi energy. The data were acquired with the INDRA detector at the GANIL (Caen, France) facility.

**Purpose:** We aim to determine the reaction and fusion cross sections for the reactions induced by  $^{129}\text{Xe}$  projectiles on  $^{\text{nat}}\text{Sn}$  targets for incident energies ranging from 8A to 35A MeV. In particular, the evaluation of the fusion and incomplete fusion cross sections is the main purpose, altogether with the comparison with the systematics of Eudes *et al.* [*Europhys. Lett.* **104**, 22001 (2013)].

**Method:** The reaction cross sections are evaluated at each beam energy with data acquired thanks to the INDRA  $4\pi$  array. The events are sorted with the help of the observable  $E_{\text{iso,max}}$ . We focus therefore our study on a selected sample of events, in such a way that the fusion and incomplete fusion cross sections can be estimated.

**Results:** We present the excitation function of reaction and fusion cross sections for the heavy and nearly symmetric system  $^{129}\text{Xe} + ^{\text{nat}}\text{Sn}$  from 8A to 35A MeV. For the fusion excitation function the comparison with the systematics of Eudes *et al.* seems to be in a fair agreement starting from the beam energy 20A MeV. For the lower beam energies (8A and 12A MeV) discrepancies are observed.

**Conclusions:** The evaluated fusionlike cross sections show a good agreement with a recent systematics for beam energies greater than 20A MeV. For low beam energies the cross-sectional values are lower than the expected ones. A probable reason for these low values is in the fusion hindrance at energies above or close to the barrier.

DOI: 10.1103/PhysRevC.94.044611

## I. INTRODUCTION

Collisions between heavy ions at low energy above the barrier are dominated by binary inelastic collisions [1–5]. According to the prediction of the classical potential model of Bass, applied to the fusion of heavy nuclei, the limiting value for fusion is given for projectile and target combinations whose product  $Z_p Z_t$  is not too large ( $Z_p Z_t \leq 2500\text{--}3000$ ) [6,7]. In this case the attractive pocket in the internuclear potential still prevents, for angular momentums  $l \leq l_{\text{crit}}$ , the reseparation of the dinuclear system, allowing it to evolve toward a compact shape, and fusion occurs, leading to compound nuclei with  $Z \leq Z_p + Z_t$ . The experimental signature of fusion processes consists in the presence of evaporation residues and fission fragments in the exit channel. For increasing projectile mass, the critical angular momentum increases. It can reach values larger than the one at which the fission barrier of the compound nucleus vanishes [6,8]. As a consequence, the fusion cross section is expected to fall to a negligible fraction [9,10] since the Coulomb repulsion dominates and the potential well is not able to trap the colliding nuclei and lead the system towards fusion anymore.

Therefore, one expects, as main exit channels, very dissipative collisions [11–13] and, with a reduced probability, fusion followed by emission of two fragments. In Deep Inelastic Collisions (DIC) the projectile and the target are strongly slowed down. During the formation of a dinuclear system and before the reseparation, nucleons may be exchanged. The process lifetime (shorter than the compound nucleus formation one) is deduced from the rotation angle of this system before decay and the dissipated energy is function of the rotation angle [14].

Experimentally it was observed that the fission cross section was greater than the upper bound imposed by the presence of the minimum in the ion-ion potential [15]. Moreover, the fission mass distributions were wider than expected on the basis of the compound nucleus model [16,17]. Therefore, part of the cross section was ascribed to fusionlike processes characterized as “fission without barrier”, which did not proceed through a compound formation. They are now referred to as quasifission [14,18–20]. Their interaction time is longer than the DIC phenomenon [21]. These capture reactions are practically indistinguishable from true compound fission and without the knowledge of the interaction times it is not possible to establish whether the two detected fragments were generated in a true fission process or in a fast-fission one. Moreover, studies on the fusion-evaporation cross section for near symmetric systems [22–25] provided evidence for the dynamical

\*Deceased.

suppression of complete fusion even if the suppression may in some cases be due to a reduced detection efficiency. The concept of an extra push in the interaction, conceived by Swiatecki [26–28], was necessary to allow the achievement of complete fusion. It was introduced in the interaction in the form of one-body dissipation and experimentally consists of a shift of the effective mean fusion barrier, causing fusion hindrance in heavy systems at energies around the barrier. Dynamical fusion theories based on different approaches [29,30] were able to reproduce data for fusion cross sections for reactions between nuclei nearly symmetric with medium-heavy masses ( $A \simeq 100$ ). A recent model [31] gives the probability of compound nucleus formation as composed by the probability of formation in overcoming the ion-ion barrier all together to the probability of diffusion toward a spherical shape from the dinuclear initial stage.

For incident energies at 10 or more MeV/nucleon above the barrier, the appearance of pre-equilibrium nucleon emission gives rise to incomplete fusion processes, leading to formation of compound nuclei with  $A < A_p + A_t$ . Moreover, since for higher beam energies more energy is converted into excitation energy, events with three or four fragments in the exit channel may constitute an important fraction of the associated cross section.

INDRA [32–35] has been used to perform a large body of measurements of the  $^{129}\text{Xe} + ^{\text{nat}}\text{Sn}$  system over a wide range of energies. This gave us a unique opportunity for an important and exclusive study of reaction mechanisms for such a heavy quasymmetric system.

Previous works on data acquired with INDRA and concerning the same system at around and above Fermi energies [36–67] focused mostly on the multifragmentation of a composite system formed in central collisions. In this paper we study the energy range from just above the barrier (8 MeV/nucleon) to the Fermi energy domain (35 MeV/nucleon). First, total reaction cross sections are determined as a function of incident energy and compared with existing systematics. Then we present a new method to estimate the total cross section for both complete or incomplete fusion and capture reactions leading to fast or quasifission. The resulting excitation function is compared with the recent systematics of Ref. [68].

## II. THE EXPERIMENT

The present study concerns the analysis of the data recorded during the fifth INDRA campaign for reactions induced by  $^{129}\text{Xe}$  projectiles on self-supporting  $350 \mu\text{g}/\text{cm}^2$  thick  $^{\text{nat}}\text{Sn}$  targets at different beam energies  $E_{\text{beam}}/A = 8, 12, 15, 18, 20, 25, 27, 29, \text{ and } 35$  MeV.

The experiment was performed at the Ganil facility (Caen, France). Since the coupling of two main cyclotrons (CSS1 and CSS2) did not allow us to explore the whole incident energy range, the  $^{129}\text{Xe}$  beam was first accelerated at 27 A MeV and successively degraded, through carbon foils of different thickness, to the energies of interest. The charge state of the primary beam was 40+. After the degrader, as expected, the Xe beam had a wide distribution of charge states. Therefore, with the help of the  $\alpha$  spectrometer, only one charge state was selected. The  $B\rho$  setting of the spectrometer was optimized

TABLE I. Kinematic characteristics for the  $^{129}\text{Xe} + ^{\text{nat}}\text{Sn}$  system at different incident energies. The laboratory velocity  $v_{\text{Lab}}$  and the center-of-mass velocity  $v_{\text{c.m.}}$  are in (cm/ns).

$E_{\text{Beam}}/A$ (MeV)	$E_{\text{c.m.}}$ (MeV)	$E_{\text{c.m.}}/V_C$	$v_{\text{Lab}}$	$v_{\text{c.m.}}$	$\Theta_{\text{gr}}^\circ$
8	494.6	1.8	3.90	2.04	22.13
12	741.6	2.7	4.77	2.50	12.84
15	926.6	3.4	5.32	2.79	9.79
18	1111.5	4.0	5.81	3.05	7.91
20	1234.6	4.5	6.12	3.21	7.02
25	1542.3	5.6	6.81	3.59	5.47
27	1665.2	6.0	7.07	3.73	5.03
29	1788.1	6.5	7.31	3.86	4.65
35	2156.3	7.8	8.00	4.23	3.80

for each incident energy. However, at low energy, more than one charge state was transmitted and this affected the incident energy with uncertainties around  $\Delta E \simeq 1$  MeV for the beam energies at 8A and 12A MeV. The energies at 29A and 35A MeV were obtained by direct tuning.

INDRA is a charged-particle multidetector covering 90% of the total solid angle. It is composed of 336 independent telescopes arranged in 17 rings centered on the beam axis. In the first ring ( $2^\circ$  and  $3^\circ$ ) are arranged 12 telescopes composed of a  $300\text{-}\mu\text{m}$  silicon wafer and a CsI(Tl) scintillator crystal (14 cm thick). Rings 2 to 9 ( $3^\circ$  to  $45^\circ$ ) have 12 or 24 three-stage detection telescopes: a gas-ionization chamber (filled with  $\text{C}_3\text{F}_8$ ), a 300- or a  $150\text{-}\mu\text{m}$  silicon wafer, and a CsI(Tl) scintillator (14 to 10 cm thick) coupled to a photomultiplier tube. Rings 10 to 17 ( $45^\circ$  to  $176^\circ$ ) are composed of 24, 16, or 8 two-member telescopes: a gas-ionization chamber and a CsI(Tl) scintillator 8, 6, or 5 cm thick. More detailed descriptions may be found in Refs. [32–35].

INDRA can measure ion charge and energy in a wide range and can resolve masses up to  $Z = 4$ . The charge identification was realized by means of the  $\Delta E$ - $E$  matrices, which well reproduce the form of the lines for each atomic number,  $Z$ . Unit charge resolution was obtained for all nuclei produced in this reaction. The energy identification threshold is  $\simeq 0.8$ – $1$  MeV/nucleon for light fragments and around  $\simeq 1.5$ – $1.7$  MeV/nucleon for fragments of  $Z = 50$ .

Collision data for the  $^{129}\text{Xe} + ^{\text{nat}}\text{Sn}$  system at the various beam energies were recorded with an acquisition trigger requiring 1, 2, 3, or 4 fired telescopes in coincidence.

Table I shows the reaction kinematic characteristics for all beam energies. The Coulomb barrier for this system at interaction radius amounts to  $V_{\text{Coul}} \simeq 275$  MeV. As it appears from the ratio of the available energy in the center of mass  $E_{\text{c.m.}}$  to the Coulomb barrier  $E_{\text{c.m.}}/V_{\text{Coul}}$ , in the third column of Table I, all the reactions take place well above the barrier.

## III. REACTION CROSS SECTION

The total reaction cross section may be defined as the total cross section minus the elastic scattering contribution:

$$\sigma_R = \sigma_T - \sigma_{\text{el}}. \quad (1)$$

TABLE II. Experimental and theoretical reaction cross sections in barns for each beam energy in MeV/nucleon.

$E_{\text{Beam}}/A$ (MeV)	$\sigma_r^{\text{Exp.}}$	$\sigma_r^{\text{Bass}}$	$\sigma_r^{\text{Kox87}}$	$\sigma_r^{\text{Tripathi}}$	$\sigma_r^{\text{Shen}}$
8	$3.96 \pm 0.70$	2.73	2.89	3.15	3.62
12	$4.87 \pm 0.30$	3.87	4.38	4.77	5.02
15	$5.26 \pm 0.30$	4.32	4.97	5.28	5.56
18	$5.59 \pm 0.38$	4.63	5.37	5.60	5.90
20	$5.62 \pm 0.47$	4.78	5.57	5.73	6.04
25	$5.82 \pm 0.39$	5.05	5.92	5.95	6.29
27	$6.15 \pm 0.26$	5.13	6.03	6.00	6.30
29	$6.36 \pm 0.24$	5.20	6.12	6.04	6.34
35	$6.51 \pm 0.59$	5.36	6.33	6.11	6.44

In order to deduce the experimental reaction cross sections, data with trigger multiplicity  $M \geq 1$  were analyzed and, under appropriate constraints, the elastic peak was isolated for each beam energy in order to evaluate the elastic scattering cross section to be subtracted in Eq. (1) from the total cross section (see  $\Theta_{gr}^\circ$  in Table I). This latter was computed as follows:

$$\sigma_T = \frac{N_{\text{event}}}{N_t I}, \quad (2)$$

where  $N_{\text{event}}$  is the total number of recorded events,  $N_t$  is the nuclear density of the target, and  $I$  is the incident flux, particles per unit time, expressed as

$$I = F \frac{(1 - \tau)}{qe}. \quad (3)$$

Here  $F$  is the charge measured by the Faraday cup,  $\tau$  is the acquisition dead time expressed as a fraction of the total acquisition time,  $q$  is the equilibrium value of the projectile charges evaluated using Ref. [69], and  $e$  is the elementary charge.

The experimental reaction cross section values obtained with this procedure are reported in Table II and displayed in Fig. 1(a). As one can see, they show a rapid increase with beam energy up to 20A MeV and then tend toward an asymptotic limit close to a purely geometrical cross section.

The associated error bars are mainly due to the uncertainties of the charge state for each incident energy. They reflect also the difficulty in some cases to accomplish a proper definition of the elastic peak. In particular, for the beam energy 35A MeV the error bars are larger because the elastic peak was mostly lost as consequence of the small grazing angle (see  $\Theta_{gr}^\circ$  in Table I). The error bars associated to the beam energy are also shown for 8A and 12A MeV.

In Fig. 1(b) the experimental reaction cross sections were normalized to the ones obtained by different theoretical parametrizations from Bass [70], Kox [71], Tripathi [72], and Shen [73] reported in Table II. The Bass parametrization was deduced in the classical framework of the strong absorption model and does not contain any mechanism of energy dissipation. As can be seen from the figure, this parametrization can constitute a lower bound for the reaction cross section of our system while the one labeled Kox84 can be considered as an upper bound (see also Table II). The

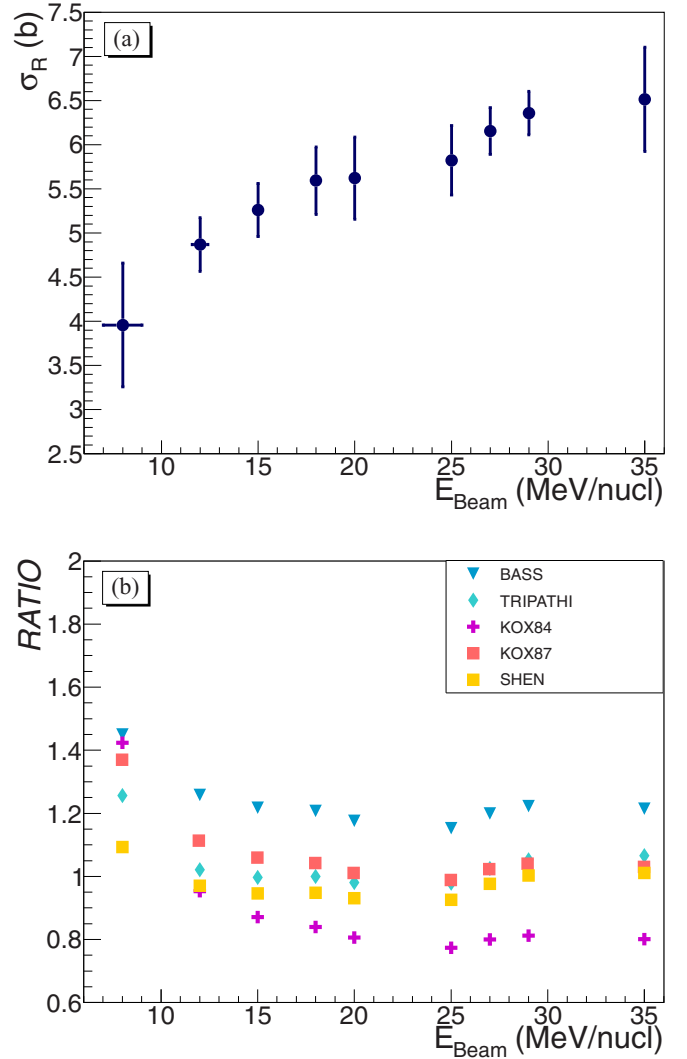


FIG. 1. (a) Experimental reaction cross sections for all beam energies. (b) Experimental reaction cross sections normalized to the theoretical values of the following parametrizations: Bass [70], Kox [71], Tripathi [72], and Shen [73].

best agreement with data is found for those parametrizations (labeled in the figure as Kox87, Tripathi, and Shen) in which were introduced corrections for the neutron excess skin [71] and for the transparency and the Pauli blocking [72]. The parametrization in Shen *et al.* [73] uses a unified formula from low to intermediate energies. It will be used when computing the fusion cross section for normalization as in Ref. [68] for comparison.

#### IV. FUSION AND INCOMPLETE FUSION CROSS SECTION EVALUATION

In this section we will evaluate the fusion cross section for the collision system at all incident energies. We discuss the global observable  $E_{\text{iso,max}}$  and the selected data with suitable characteristics for the cross-sectional evaluation. A comparison with the analysis in Ref. [68] will also be discussed.

### A. Observable $E_{\text{iso,max}}$

In order to select classes of events with marked fusion characteristics,

the kinematic global observable  $E_{\text{iso,max}}$  [66,74] in term of the velocity components of the heaviest fragment in the event was used. This observable is defined as

$$E_{\text{iso,max}} = V_{\parallel,\text{max}}^2 - 0.5V_{\perp,\text{max}}^2(1 + \sin 2\phi), \quad (4)$$

where  $V_{\parallel,\text{max}}$  and  $V_{\perp,\text{max}}$  are the velocity components of the heaviest fragment in the center of mass (c.m.) parallel and orthogonal to the beam direction and  $\phi$  is its azimuthal angle.

The  $E_{\text{iso,max}}$  observable enhances the separation between the projectile-like contributions and the more damped events whose products are produced at rest in the -of-mass frame. Figure 3(a) shows the result of a simulation in which fragments have an isotropic momentum distribution in the center-of-mass frame [75]. The resulting distribution of  $E_{\text{iso,max}}$  is symmetric around zero, even for events with only two fragments (fission-like events). If the source of emission is not at rest in the center-of-mass frame, but moves with a moderate velocity ( $\leq 1$  cm/ns), either more quickly or more slowly than the center-of-mass frame (such as in the case of incomplete fusion), the distribution is still peaked at zero but skewed toward positive values of  $E_{\text{iso,max}}$ , in such a way that the total number of events with  $E_{\text{iso,max}} < 0$  MeV/nucleon is less than 50% of the total. A similar effect is observed for a nonisotropic emission pattern at rest in the center of mass. On the other hand, for larger source velocities in the c.m. frame (such as for projectile-like decays), the whole distribution is shifted to positive values without a pronounced peak and there are no longer any events for which  $E_{\text{iso,max}} < 0$  MeV/nucleon. Therefore, the measured cross section for  $E_{\text{iso,max}} < 0$  MeV/nucleon can be considered as a lower limit for the cross section for capture reactions (fusion-evaporation, fusion-fusion, quasifission), with a negligible contribution from binary dissipative collisions. A simulation on the present collision system for central events with the code SMM [76] gave the same pattern [74] as in Fig. 3(b).

In Fig. 2 is shown the experimentally measured correlation between  $E_{\text{iso,max}}$  and the quantity  $\sqrt{E_{\text{LLCP}}}$  for 15A MeV bombarding energy.  $\sqrt{E_{\text{LLCP}}}$  is the square root of the total transverse energy of light charged particles ( $Z < 3$ ) and is related to the degree of centrality of the collision [77,78]. One can identify two components, separated by the black line in the figure at  $E_{\text{iso,max}} \simeq 2$  MeV/nucleon. The first (labelled with A) is the component with  $E_{\text{iso,max}} < 2$  MeV/nucleon. The second, for values  $E_{\text{iso,max}} > 2$  MeV/nucleon, comprises the two zones labeled with B and C. These two components indicate clearly an evolution of the dissipated energy from central to peripheral collisions. The deep valley observed close to  $E_{\text{iso,max}} \simeq 2$  MeV/nucleon helps to accomplish the separation between binary (deep inelastic collisions, DIC) and central collisions (candidate for fusion).

Figure 3(b) shows the experimental observable  $E_{\text{iso,max}}$  for the collision at 15A MeV. This correlation is not symmetric around zero since it contains all the reaction contributions. To guide the eye the negative part was reversed and superposed to the positive one. According to the results of the simulation

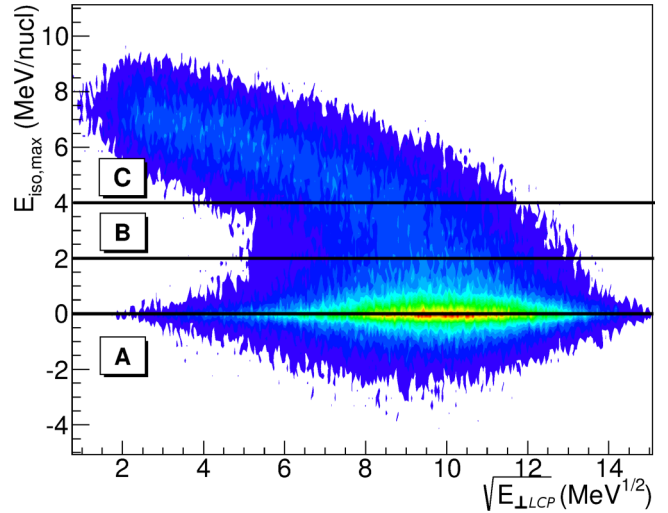


FIG. 2.  $E_{\text{iso,max}}$  vs  $\sqrt{E_{\text{LLCP}}}$  for the system at 15A MeV.  $E_{\text{iso,max}}$  appears subdivided in three zones: A, B, and C. See text for details.

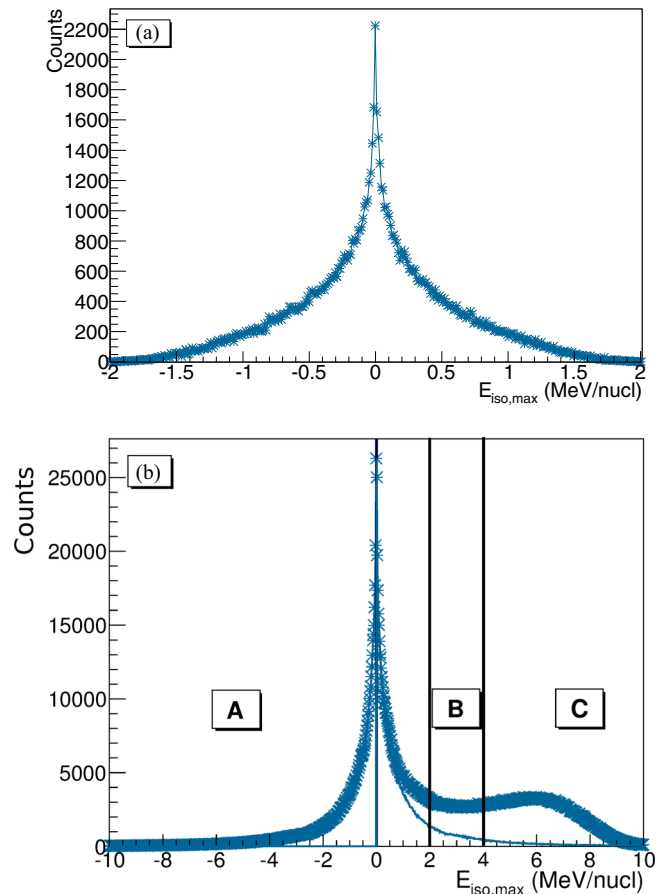


FIG. 3. (a) Simulation of  $E_{\text{iso,max}}$  for pure central collisions with unique source formation. In this case the observable is perfectly symmetric around zero [74,75]. (b) Experimental  $E_{\text{iso,max}}$  at 15A MeV. In order to appreciate this symmetry, more hidden for experimental data, the negative part has been reversed and superimposed to the positive values. The labels A, B, and C refer to the zones discussed in the text.

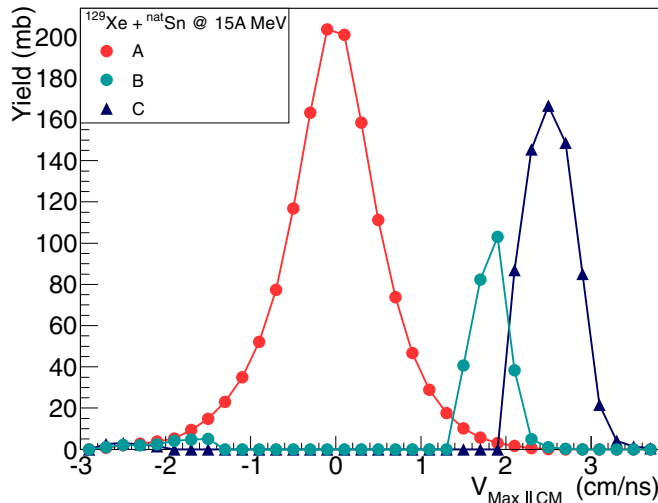


FIG. 4. Heaviest fragment CM parallel velocity for three different bins of  $E_{\text{iso,max}}$  for the system at 15A MeV. A represents event selected with  $E_{\text{iso,max}} \leq 0$  MeV/nucleon, B with  $2 \leq E_{\text{iso,max}} \leq 4$  MeV/nucleon, and C with  $E_{\text{iso,max}} > 4$  MeV/nucleon.

presented above, in the following we will estimate the fusionlike cross section by doubling the yield of events with  $E_{\text{iso,max}} < 0$  MeV/nucleon.

### B. Event selection by $E_{\text{iso,max}}$ bins

The global observable  $E_{\text{iso,max}}$  may be used to sort the events accordingly to the underlying reaction mechanism. In fact, depending on the choice of the bins in which the observable can be divided, it is possible to select roughly three classes of events: One for which the fusionlike and capture reactions are the dominant mechanism, a second resembling highly damped binary collisions, and finally events belonging to less dissipative reactions.

Figure 4 shows the longitudinal velocity distributions of the heaviest fragment for events selected according to  $E_{\text{iso,max}}$  bins values for the reaction at 15A MeV. The events labeled with A were selected via  $E_{\text{iso,max}} \leq 0$  MeV/nucleon and doubled. In this case the distribution is Gaussian and symmetric around zero and groups fusion events. The distribution labeled with B is formed by events selected with  $2 \leq E_{\text{iso,max}} \leq 4$  MeV/nucleon and is subdivided into two asymmetric bumps. These two bumps should actually have the same size, but due to identification thresholds at backward angles for the slow-moving quasitarget, the latter gives just a very small bump at negative center-of-mass velocities. The third component, for  $E_{\text{iso,max}} > 4$  MeV/nucleon, is close to the beam velocity, indicating collisions with little dissipation, for which the quasiprojectile (QP) was detected.

Figure 5 shows, for the same bins of  $E_{\text{iso,max}}$  as in Fig. 4, the charge distributions of the heaviest fragment expressed in millibarns. As before, selection A gives the charge distribution for the heaviest fragment for the fusionlike events. From this distribution it is clear that the condition  $E_{\text{iso,max}} \leq 0$  MeV/nucleon selects also events without fragments (in this work are named fragments nuclei with charge greater than

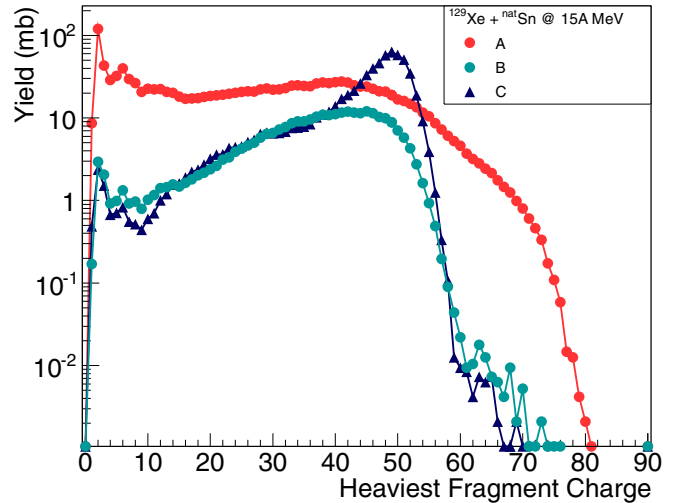


FIG. 5. Heaviest fragment charge for bins of  $E_{\text{iso,max}}$  as Fig. 4 for 15A MeV. The yields are expressed in mb.

10). This means that events just constituted by light charged particles and intermediate-mass fragments (IMF) with charge  $3 \leq Z \leq 9$  are also included. In these events the heaviest fragment can be a proton, an  $\alpha$ , or an IMF. At low excitation energies these events are issued by evaporation from the composite system or by one of the two partners in a DIC event. The condition  $E_{\text{iso,max}} \leq 0$  MeV/nucleon applied to these events is able to select properly the fusion events. Moreover, until 18A MeV, the events selected either with zero fragment multiplicity or with both conditions,  $E_{\text{iso,max}} \leq 0$  MeV/nucleon and zero fragment multiplicity, do not differ too much, since the nonfusion contribution is small. Starting from 20A MeV, a larger number of IMF is produced from neck fragmentation [79]. As a consequence, the events with no fragments show a velocity distribution more centered around very low velocities (one can speculate that these light charged particles are mostly coming from the target evaporation). The selection  $E_{\text{iso,max}} \leq 0$  MeV/nucleon still selects fusion events but the velocity distributions are not any more Gaussian: They are slightly asymmetric toward lower velocities. This contribution may be removed, placing a further constraint on the heaviest fragment charge, as it will be explained in the next paragraph.

Figure 6 shows the correlation of the heaviest and second heaviest fragment charges for events with two fragments in the exit channel. In Fig. 6(a) the correlation is without selection on  $E_{\text{iso,max}}$ . Figure 6(b) shows the correlation for  $E_{\text{iso,max}} \leq 0$  MeV/nucleon. The constraint on the global variable selects therefore events in which the two fragments result from the scission of a composite system with  $Z_1 + Z_2 \simeq 75-80$ . In fact the lower ridge of Fig. 6(a) corresponds to events having a relative folding angle which is around  $90-100^\circ$  while the higher ridge, which is more evident in Fig. 6(b) after the selection with  $E_{\text{iso,max}} \leq 0$  MeV/nucleon, has a relative folding angle centered at  $160^\circ$ , close to back-to-back emission.

Figure 7 shows the same selection applied to the Wylczinski plot: Fragment total kinetic energy (TKE) as a function of the flow angle [12,13,80]. The selection condition applied to data in the lower panel, Fig. 7(b) selects mainly events with a small

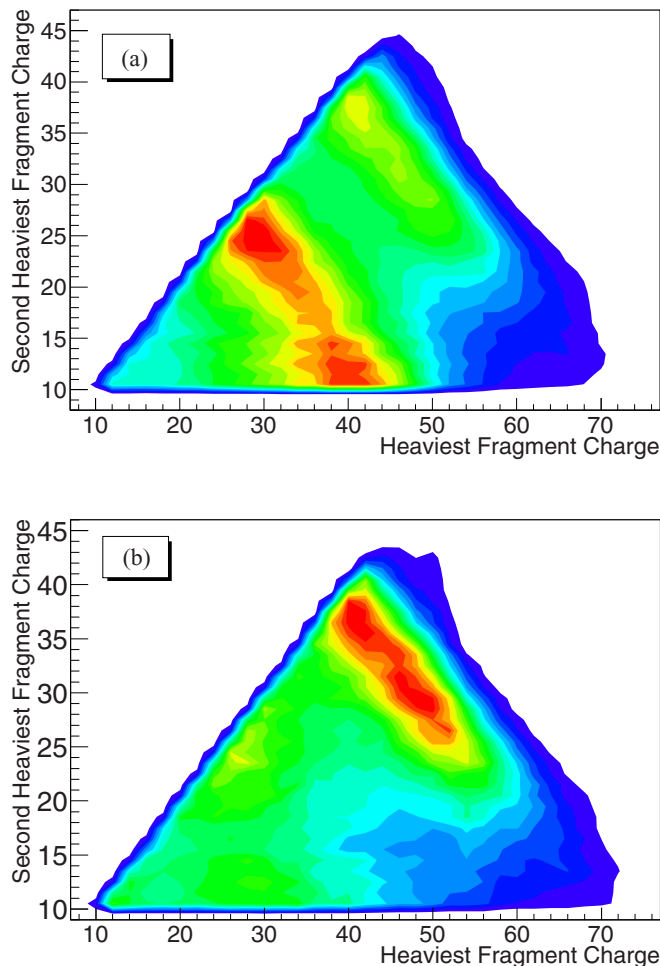


FIG. 6. Correlation of the second heaviest fragment charge with the heaviest fragment charge for the system at 15A MeV for events with two fragments in the exit channel. (a) No selection on  $E_{iso,max}$ . (b)  $E_{iso,max} \leq 0$

TKE and a near-isotropic distribution of flow angles (peaked at  $\Theta_{flow} \simeq 90^\circ$ ). It should be noted that the TKE distribution is peaked between the values expected for symmetric fission of composite systems with  $Z_1 + Z_2 \simeq 75 - 80$  (TKE  $\simeq 140$  MeV) and  $Z_1 + Z_2 = 104$  (TKE  $\simeq 200$  MeV) [81].

We conclude this paragraph showing, in Fig. 8, the charge distributions for each incident energy. In this figure, the distributions were weighted in order to give the cross-sectional fraction pertinent to each beam energy and then normalized to the event number. The  $E_{iso,max} \leq 0$  MeV/nucleon selection was also applied.

### C. Fusion cross section evaluation

In this paragraph the attention will be focused on fusion and incomplete fusion reactions. We will evaluate the experimental fusion cross sections by using the condition  $E_{iso,max} \leq 0$  MeV/nucleon alone or adding one more constraint and then doubled. The values of the fusion and incomplete fusion cross sections found in our analysis will be compared to the predictions of Ref. [68] in which a function was deduced from

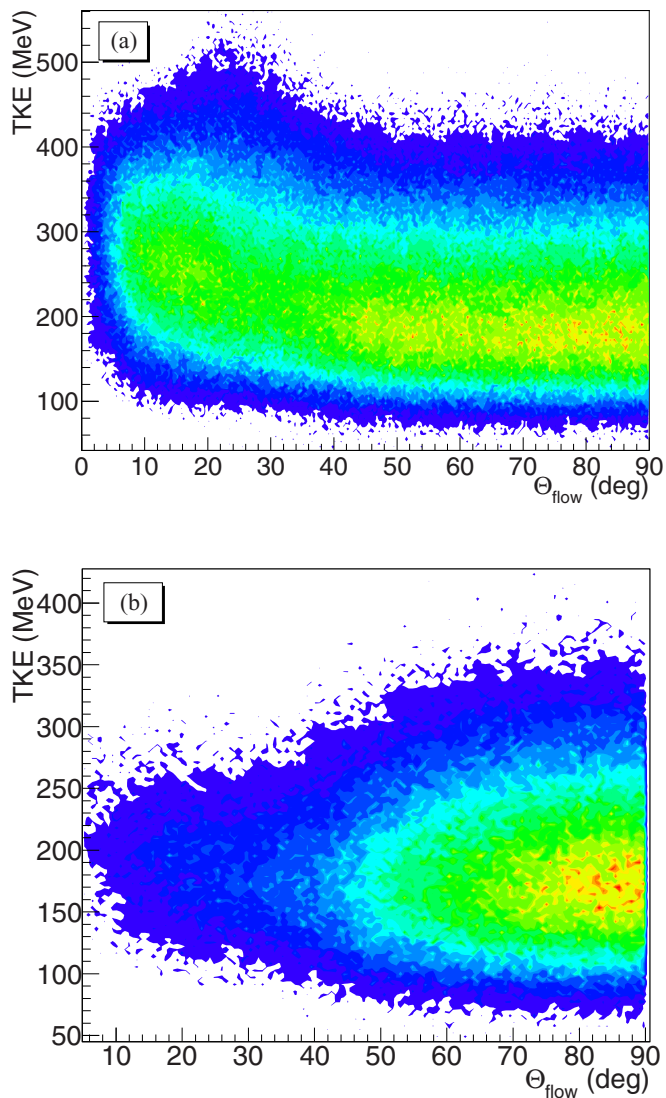


FIG. 7. Total kinetic energy versus flow angle for the system at 15A MeV for events with two fragments in the exit channel. (a) No selection on  $E_{iso,max}$ . (b)  $E_{iso,max} \leq 0$  MeV/nucleon.

an experimental systematics based on the mass asymmetry parameter.

To estimate the fusion and incomplete fusion cross section, we also need to account for those events for which not all the particles were completely detected. An initial selection based only on the computation of complete events would have drastically excluded all the events where the residue or one of the fission fragments was lost. Consequently it was argued more correct to select fusion events by the condition  $E_{iso,max} \leq 0$  for the reasons discussed above. These events were then doubled according to the symmetry of the observable. We did, however, require that the heaviest fragment of each event was identified in either the ionization chamber silicon telescopes ( $\theta \leq 45^\circ$ ) or in the ion chamber CsI telescope ( $\theta > 45^\circ$ ), which excludes most events where the heaviest fragment is a light charged particle ( $Z \leq 2$ ).

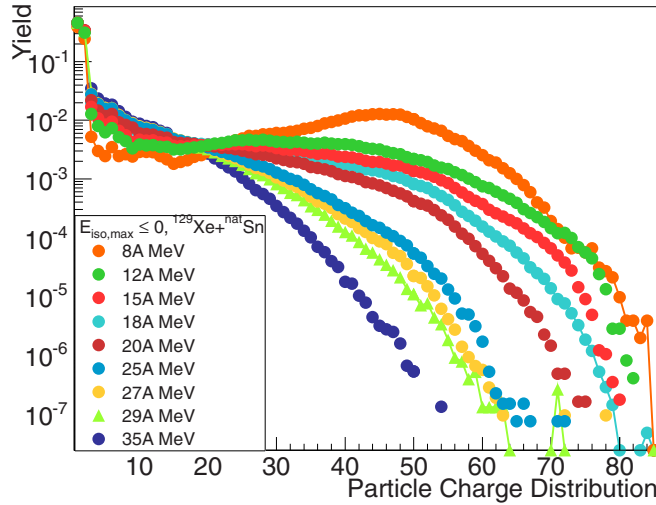


FIG. 8. Particle charge distributions at all beam energies. See text for details.

Starting from  $E_{\text{Beam}} = 18A$  MeV up to  $E_{\text{Beam}} = 35A$  MeV we added also a constraint on the heaviest fragment charge to reject events with increasing IMF multiplicities coming from the neck emission. Figures 9 and 10 help to demonstrate this point. Figure 9 shows the heaviest fragment charge versus the  $E_{\text{iso,max}}$  at 18A MeV. In this figure one can observe three bumps: one for peripheral events, one for fusion events, and one mostly constituted by events in which the heaviest fragment has a very low charge because the true one was not detected. Figure 10 shows the heaviest charge distributions for beam energies from 18A to 35A MeV expressed in mbarns. The condition  $E_{\text{iso,max}} \leq 0$  MeV/nucleon was applied. One can remark minima in the heaviest charge are evident, with a greater increase for higher energies. On the basis of this

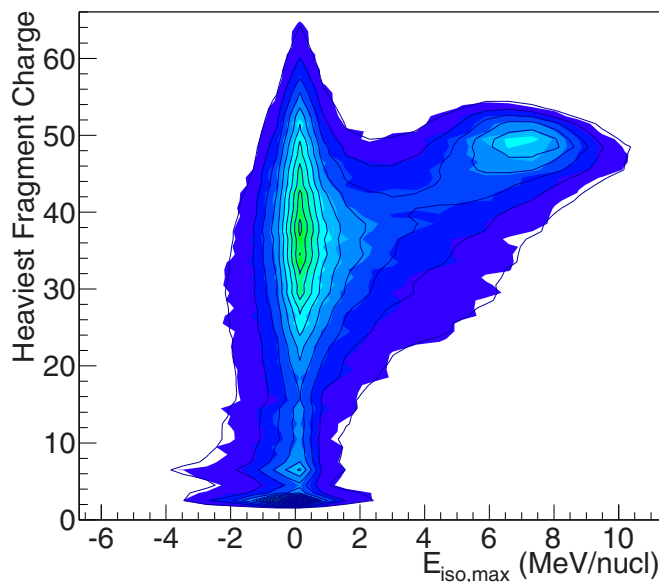


FIG. 9. Correlation for the heaviest fragment charge vs  $E_{\text{iso,max}}$  for  $E_{\text{Beam}} = 18A$  MeV.

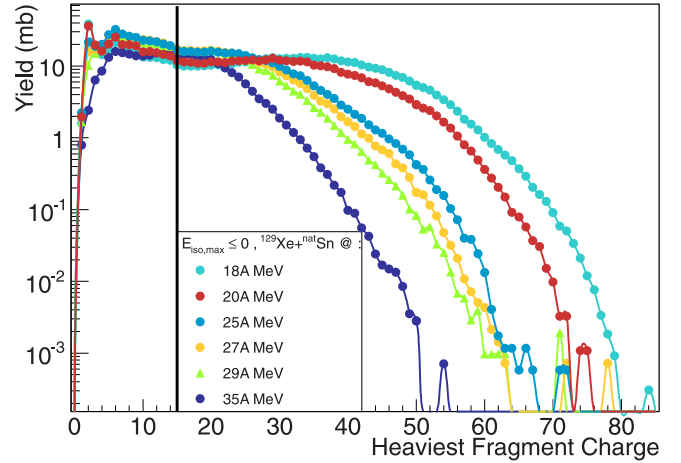


FIG. 10. Heaviest fragment charge at incident energies 18A to 35A MeV with the  $E_{\text{iso,max}} \leq 0$  MeV/nucleon selection. The vertical black line gives the cut at  $Z_{\text{max}} = 15$ .

feature it was considered as a better choice to accept events whose the heaviest fragment charge was larger than a certain limit, deduced from Fig. 10. This limit, actually the same for each beam energy, was set at  $Z_{\text{max}} \geq 15$ . In this way the contribution from the neck emission was minimized.

The fusion cross sections computed with these selections are shown in Table III. The error bars were evaluated by computing the cross section value corresponding to different selections on the heaviest charge for higher beam energies. For lower energies it was useful to study the set composed by events without any fragment and compute the cross section values with and without this set.

No correction for efficiency has still been applied: This could influence the cross-sectional results, especially for low bombarding energies, where the compound formation may travel directly in the very forward direction without being detected. However, this effect should be more dramatic as the beam energy increases since all the products are more focused in the forward direction.

The fusion cross-sectional values of Table III are shown in Fig. 11(a). These values show a maximum at 15A MeV. One expects that for the beam energies of 8A and 12A MeV the values of the cross sections are higher. Even if for 8A MeV the fusion hindrance, discussed above, would diminish the

TABLE III. Fusion cross section values in mb.

$E_{\text{beam}}$ (MeV/nucleon)	$\sigma_{\text{Fus/IF}}$ (mb)
8	$390 \pm 50$
12	$752 \pm 130$
15	$1100 \pm 100$
18	$900 \pm 110$
20	$790 \pm 100$
25	$590 \pm 100$
27	$550 \pm 80$
29	$490 \pm 80$
35	$290 \pm 60$

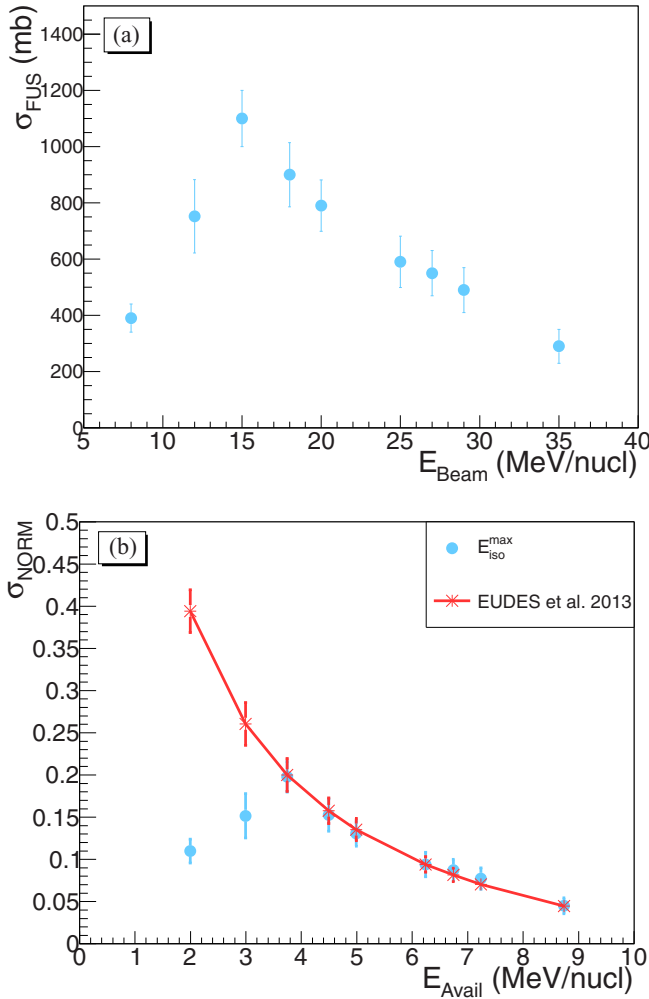


FIG. 11. (a) Experimental fusion cross section. (b) Fusion cross section normalized for the Shen total reaction cross section.

fusion probability; the detector acceptance is suspected to be responsible for the loss of fusion and incomplete fusion events since all the residues with a forward angle lower than  $3^\circ$  were lost. For increasing energies the probability for fusion events decreases rapidly: At higher energies the transparency effects of the nuclear matter dominate, as was observed in Refs. [61,65]. Because of its high kinetic energy the incident nucleus cannot any longer succeed in forming a compound nucleus with the target and both are broken in several fragments during the collision.

Figure 11(b) shows the cross section values normalized to Shen's [73] values of the total reaction cross section previously discussed in order to compare them to those obtained for our system as described in the work accomplished by Eudes and colleagues [68], which displays a systematic study on a large body of fusion data in order to deduce a universal behavior. The different systems were organized depending on their size, taking into account the mass asymmetry, and data were plotted in function of the available energy defined as follows:

$$E_{\text{avail}} = \frac{E_{\text{lab}}}{A_{\text{proj}}} \frac{A_{\text{proj}} A_{\text{target}}}{(A_{\text{proj}} + A_{\text{target}})^2}. \quad (5)$$

The authors deduced a homographic function starting from the ratio of the fusion cross section to the reaction cross section. In the present work the red curve with star symbols in Fig. 11 is the homographic function calculated for the  $^{129}\text{Xe} + ^{\text{nat}}\text{Sn}$  system using the parameters given in Ref. [68] and  $A_{\text{target}} = 119$  for the  $^{\text{nat}}\text{Sn}$  target.

As one can see from Fig. 11, the cross sections values are in fairly good agreement with the function from Eudes *et al.* Although the homographic function in Ref. [68] was deduced for light to intermediate systems and then extrapolated to heavy systems it seems to work fairly well also for this heavy system. On the red curve one can see the expected values for 8A and 12A MeV. These two lowest bombarding energies are the closest to the barrier and it would be important to understand if their cross sections are hindered because of the lower incident energy. Preliminary insight came recently [82]. A first simplified simulation based on the two-step model [83,84] applied to the system at 8A and 12A MeV beam energies (for  $J = 0 \hbar$ ) gave fusion cross sections in agreement with the experimental ones above reported. The question is still studied in order to take in account correctly the angular momentum.

## V. DISCUSSION AND CONCLUSIONS

In this work the energy dependence of the experimental reaction cross section was displayed and compared to different parametrizations. Data were found in fair agreement with those which take into account the effects due to the neutron skin and Pauli blocking [73].

Then we turned to the fusion cross-sectional evaluation for which candidates for fusion events were selected with the help of the  $E_{\text{iso,max}}$  observable. It is the first time that such a study is accomplished, for a wide energy range from 8A to 35A MeV, on the quasisymmetric heavy system  $^{129}\text{Xe} + ^{\text{nat}}\text{Sn}$ .

The excitation function obtained shows a maximum around 15A MeV and then falls to lower values at increasing energies. Values of the same order can be found in the literature for mass intermediate systems and for lower bombarding energies [8] or light systems at comparable energies (Ref. [55] and references therein).

For heavy colliding nuclei the compound system formed decays by fission, which become the favorite exit channels depending on the fissility of the compound system  $Z^2/A$ . Since in the diabatic hindrance model starting from a fusibility parameter  $x_m = 0.75$  [30,85] fusion becomes a dynamically hindered process, for  $^{129}\text{Xe} + ^{\text{nat}}\text{Sn}$  with  $x_m \simeq 9$ , fission and quasifission are clearly in competition.

As we discussed and showed, our method of computing the fusion cross section succeeds in excluding the DIC component. It is clear that for this system there is a quasifission component. As already discussed, this process is slower than the DIC and does not proceed through the compound nucleus formation. To quantify it one should determine the characteristic decay times from angular distributions or solve isotopically the detected fragments [14]. This was beyond our purpose, which was merely to supply a fusion upper bound for this system in particular, scaling with the beam energies. However, in the future, FAZIA [86] could be able to detect the fragments with

a good isotopic resolution and so could be able to disentangle the different fusionlike mechanisms.

The fusion cross sections of Table III were compared to a theoretical curve expected to give a universal behavior. For all the energies but the lower ones (8A and 12A MeV), a nice agreement was found with the universal behavior found by Eudes *et al.* [68]. More data on quasisymmetric and heavy systems would help to support the results of the present study. The selection with the  $E_{\text{iso,max}}$  observable was powerful in separating the different contributions for central, semiperipheral, and peripheral events. In particular, the sample of semiperipheral collisions show few characteristics of deep inelastic collisions, as shown displayed in the text.

As already mentioned, the evident discrepancy from the general trend for lower energies (8A and 12A MeV) could be ascribed to the intrinsic difficulty (the second inner fusion barrier needing an extra push of energy to be overcome) for heavy elements to form a true compound nucleus. The acceptance of INDRA at very low angles (lower than  $3^\circ$ ) complicates the analysis because of the loss of those residues ejected in the very forward direction and only slightly deviated by the light particle evaporation process. To better understand and clarify this point, simulations with a Monte Carlo code are needed. In particular, simulations with the codes HIPSE [87] and GEMINI [88,89] are currently in progress in order to better understand the roles both of INDRA acceptance and of fusion hindrance. They will constitute the subject of a forthcoming article.

- 
- [1] W. U. Schröder and I. R. Huizenga, *Treatise on Heavy Ion Science*, edited by A. Bromley (Plenum Press, New York, 1984), Vol. 2.
- [2] P. Glässel *et al.*, *Z. Phys. A* **310**, 189 (1983).
- [3] A. A. Stefanini *et al.*, *Z. Phys. A* **351**, 167 (1995).
- [4] R. J. Charity *et al.*, *Z. Phys. A* **341**, 53 (1991).
- [5] J. Wilczyński *et al.*, *Phys. Rev. C* **81**, 067604 (2010).
- [6] R. Bass, *Nucl. Phys. A* **231**, 45 (1974).
- [7] C. Ngô *et al.*, *Nucl. Phys. A* **240**, 353 (1975).
- [8] B. Tamain, C. Ngô, J. Peter, and F. Hanappe, *Nucl. Phys. A* **252**, 187 (1975).
- [9] U. Mosel, in *Treatise on Heavy-Ion Science*, Vol. 2 (Plenum, New York, 1984).
- [10] M. Lefort and Ch. Ngô, *Ann. Phys. Fr.* **3**, 5 (1978).
- [11] W. U. Schroeder and J. R. Huizenga, *Treatise on Heavy-Ion Science* (Plenum, Bromley, New York, 1984).
- [12] J. Wilczyński, *Phys. Lett. B* **47**, 124 (1973).
- [13] J. Wilczyński, *Phys. Lett. B* **47**, 484 (1973).
- [14] J. Toke *et al.*, *Nucl. Phys. A* **440**, 327 (1985).
- [15] B. Heusch *et al.*, *Z. Phys. A* **288**, 391 (1878).
- [16] B. Borderie, M. Berlinger *et al.*, *Z. Phys. A* **299**, 263 (1981).
- [17] B. B. Back, H. Esbensen, C. L. Jiang and K. E. Rehm, *Rev. Mod. Phys.* **86**, 317 (2014).
- [18] J. Péter, C. Ngô, F. Plasil, M. Berlinger, and F. Hanappe, *Nucl. Phys. A* **279**, 110 (1977).
- [19] M. G. Itkis *et al.*, in *2001 Proceedings of the International Conference on Fusion Dynamics at the Extremes (Dubna)*, edited by Yu. Ts. Oganessian and V. I. Zagrebaev (World Scientific, Singapore, 2000), pp. 93–109.
- [20] M. G. Itkis *et al.*, *Nucl. Phys. A* **734**, 136 (2004).
- [21] V. Zagrebaev and W. Greiner, *J. Phys. G: Nucl. Part. Phys.* **31**, 825 (2005).
- [22] C.-C. Sahn *et al.*, *Z. Phys. A* **319**, 113 (1984).
- [23] J. G. Keller *et al.*, *Nucl. Phys. A* **452**, 173 (1986).
- [24] W. Morawek *et al.*, *Z. Phys. A* **341**, 75 (1991).
- [25] A. B. Quint *et al.*, *Z. Phys. A* **346**, 119 (1993).
- [26] W. J. Swiatecki, *Phys. Scr.* **24**, 113 (1981).
- [27] W. J. Swiatecki, *Nucl. Phys. A* **376**, 275 (1982).
- [28] J. P. Blocki *et al.*, *Nucl. Phys. A* **459**, 145 (1986).
- [29] A. Lukasiak, W. Cassing, and W. NoreMBERG, *Nucl. Phys. A* **426**, 181 (1984).
- [30] D. Berdichevsky *et al.*, *Nucl. Phys. A* **502**, 395 (1989).
- [31] K. Siwek-Wilczynska and J. Wilczynski, *Phys. Rev. C* **71**, 014602 (2005).
- [32] J. Pouthas *et al.*, *Nucl. Instr. Meth. A* **357**, 418 (1995).
- [33] J. Pouthas *et al.*, *Nucl. Instr. Meth. A* **369**, 222 (1996).
- [34] M. Pärlog *et al.*, *Nucl. Instr. Meth. A* **482**, 674 (2002).
- [35] M. Pärlog *et al.*, *Nucl. Instr. Meth. A* **482**, 693 (2002).
- [36] J. Lukasik *et al.*, *Phys. Rev. C* **55**, 1906 (1997).
- [37] N. Marie *et al.*, *Phys. Lett. B* **391**, 15 (1997).
- [38] N. Marie *et al.*, *Phys. Rev. C* **58**, 256 (1998).
- [39] R. Nebauer *et al.*, *Nucl. Phys. A* **658**, 67 (1999).
- [40] D. Gourio *et al.*, *Eur. Phys. J. A* **7**, 245 (2000).
- [41] M. Germain *et al.*, *Phys. Lett. B* **488**, 211 (2000).
- [42] F. Bocage *et al.*, *Nucl. Phys. A* **676**, 391 (2000).
- [43] V. Metivier *et al.*, *Nucl. Phys. A* **672**, 357 (2000).
- [44] B. Borderie, G. Tabacaru, P. Chomaz, M. Colonna, A. Guarnera, M. Parlog, M. F. Rivet, G. Auger, C. O. Bacri, N. Bellaize, R. Bougault, B. Bouriquet, R. Brou, P. Buchet, A. Chbihi, J. Colin, A. Demeyer, E. Galichet, E. Gerlic, D. Guinet, S. Hudan, P. Lattes, F. Lavaud, J. L. Laville, J. F. Lecolley, C. Leduc, R. Legrain, N. Le Neindre, O. Lopez, M. Louvel, A. M. Maskay, J. Normand, P. Pawlowski, E. Rosato, F. Saint-Laurent, J. C. Steckmeyer, B. Tamain, L. Tassan-Got, E. Vient, J. P. Wieleczko (INDRA Collaboration), *Phys. Rev. Lett.* **86**, 3252 (2001).
- [45] J. D. Frankland *et al.*, *Nucl. Phys. A* **689**, 940 (2001).
- [46] J. C. Steckmeyer *et al.*, *Nucl. Phys. A* **686**, 537 (2001).
- [47] N. Bellaize *et al.*, *Nucl. Phys. A* **709**, 367 (2002).
- [48] D. Cussol *et al.*, *Phys. Rev. C* **65**, 044604 (2002).
- [49] S. Hudan, A. Chbihi, J. D. Frankland, A. Mignon, J. P. Wieleczko, G. Auger, N. Bellaize, B. Borderie, A. Botvina, R. Bougault, B. Bouriquet, A. M. Buta, J. Colin, D. Cussol, R. Dayras, D. Durand, E. Galichet, D. Guinet, B. Guiot, G. Lanzalone, P. Lattes, F. Lavaud, J. F. Lecolley, R. Legrain, N. Le Neindre, O. Lopez, L. Manduci, J. Marie, L. Nalpas, J. Normand, M. Parlog, P. Pawlowski, M. Pichon, E. Plagnol, M. F. Rivet, E. Rosato, R. Roy, J. C. Steckmeyer, G. Tabacaru, B. Tamain, A. van Lauwe, E. Vient, M. Vigilante, C. Volant (INDRA Collaboration), *Phys. Rev. C* **67**, 064613 (2003).
- [50] J. Colin, D. Cussol, J. Normand, N. Bellaize, R. Bougault, A. M. Buta, D. Durand, O. Lopez, L. Manduci, J. Marie, J. C. Steckmeyer, B. Tamain, A. Van Lauwe, E. Vient, B. Borderie, F. Lavaud, N. Le Niendre, P. Pawlowski, E. Plagnol, M. F. Rivet, B. Bouriquet, A. Chbihi, J. D. Frankland, B. Guiot, S. Hudan, J. P. Wieleczko, J. L. Charvet, R. Dayras, L. Nalpas, C. Volant, E. Galichet, D. Guinet, P. Lattes, M. Parlog, E. Rosato, M.

- Vigilante, R. Roy (INDRA Collaboration), *Phys. Rev. C* **67**, 064603 (2003).
- [51] A. Le Fevre *et al.*, *Nucl. Phys. A* **735**, 219 (2004).
- [52] S. Piantelli *et al.*, *Phys. Lett. B* **627**, 18 (2005).
- [53] J. D. Frankland, A. Chbihi, A. Mignon, M. L. Begemann-Blaich, R. Bittiger, B. Borderie, R. Bougault, J. L. Charvet, D. Cussol, R. Dayras, D. Durand, C. Escano-Rodriguez, E. Galichet, D. Guinet, P. Loutesse, A. Le Fevre, R. Legrain, N. Le Neindre, O. Lopez, J. Lukasik, U. Lynen, L. Manduci, J. Marie, W. F. J. Muller, L. Nalpas, H. Orth, M. Parlog, M. Pichon, M. F. Rivet, E. Rosato, R. Roy, A. Saija, C. Schwarz, C. Sfienti, B. Tamain, W. Trautmann, A. Trzcinski, K. Turzo, A. Van Lauwe, E. Vient, M. Vigilante, C. Volant, J. P. Wieleczko, B. Zwieglinski (INDRA and ALADIN Collaborations), *Phys. Rev. C* **71**, 034607 (2005).
- [54] M. Pichon *et al.*, *Nucl. Phys. A* **779**, 267 (2006).
- [55] P. Loutesse *et al.*, *Eur. Phys. J., A* **27**, 349 (2006).
- [56] G. Tabacaru *et al.*, *Nucl. Phys. A* **764**, 371 (2006).
- [57] N. Le Neindre *et al.*, *Nucl. Phys. A* **795**, 47 (2007).
- [58] S. Piantelli *et al.*, *Nucl. Phys. A* **809**, 111 (2008).
- [59] A. Le Fevre *et al.*, *Phys. Lett. B* **659**, 807 (2008).
- [60] E. Bonnet *et al.*, *Nucl. Phys. A* **816**, 1 (2009).
- [61] G. Lehaut, D. Durand, O. Lopez, E. Vient, A. Chbihi, J. D. Frankland, E. Bonnet, B. Borderie, R. Bougault, E. Galichet, D. Guinet, Ph. Loutesse, N. Le Neindre, P. Napolitani, M. Parlog, M. F. Rivet, and E. Rosato (INDRA and ALADIN Collaborations), *Phys. Rev. Lett.* **104**, 232701 (2010).
- [62] E. Bonnet *et al.*, *Phys. Rev. Lett.* **105**, 142701 (2010).
- [63] B. Borderie *et al.*, *Phys. Lett. B* **723**, 140 (2013).
- [64] D. Gruyer, J. D. Frankland, R. Botet, M. Płoszajczak, E. Bonnet, A. Chbihi, G. Ademard, M. Boisjoli, B. Borderie, R. Bougault, D. Guinet, P. Loutesse, L. Manduci, N. Le Neindre, P. Marini, P. Pawłowski, M. F. Rivet, E. Rosato, G. Spadaccini, M. Vigilante, and J. P. Wieleczko (INDRA collaboration), *Phys. Rev. Lett.* **110**, 172701 (2013).
- [65] O. Lopez, D. Durand, G. Lehaut, B. Borderie, J. D. Frankland, M. F. Rivet, R. Bougault, A. Chbihi, E. Galichet, D. Guinet, M. La Commara, N. Le Neindre, I. Lombardo, L. Manduci, P. Marini, P. Napolitani, M. Prlog, E. Rosato, G. Spadaccini, E. Vient, and M. Vigilante (INDRA Collaboration), *Phys. Rev. C* **90**, 064602 (2014).
- [66] G. Ademard *et al.*, *Eur. Phys. J., A* **50**, 33 (2014).
- [67] D. Gruyer, J. D. Frankland, E. Bonnet, A. Chbihi, G. Ademard, M. Boisjoli, B. Borderie, R. Bougault, E. Galichet, J. Gauthier, D. Guinet, P. Loutesse, N. Le Neindre, E. Legouee, I. Lombardo, O. Lopez, L. Manduci, P. Marini, K. Mazurek, P. N. Nadtochy, M. Parlog, M. F. Rivet, R. Roy, E. Rosato, G. Spadaccini, G. Verde, E. Vient, M. Vigilante, J. P. Wieleczko (INDRA Collaboration), *Phys. Rev. C* **92**, 064606 (2015).
- [68] P. Eudes *et al.*, *Europhys. Lett.* **104**, 22001 (2013).
- [69] R. Schiwietz, *Nucl. Instr. Meth. B* **175-177**, 125 (2001).
- [70] R. Bass, *Nuclear Reactions with Heavy Ions* (Springer-Verlag, Berlin, 1980).
- [71] S. Kox *et al.*, *Nucl. Phys. A* **420**, 162 (1984); *Phys. Rev. C* **35**, 1678 (1987).
- [72] R. K. Tripathi, F. E. Cucinotta, and J. W. Wilson, Nasa Technical Paper 3621, 1997 (unpublished).
- [73] W. Q. Shen *et al.*, *Nucl. Phys. A* **491**, 130 (1989).
- [74] R. Bougault *et al.* (private communication).
- [75] J. D. Frankland (private communication).
- [76] A. Botvina *et al.*, *Nucl. Phys. A* **475**, 663 (1987).
- [77] L. Phair *et al.*, *Nucl. Phys. A* **548**, 489 (1992).
- [78] E. Plagnol, J. Lukasik, G. Auger, C. O. Bacri, N. Bellaize, F. Bocage, B. Borderie, R. Bougault, R. Brou, P. Buchet, J. L. Charvet, A. Chbihi, J. Colin, D. Cussol, R. Dayras, A. Demeyer, D. Dore, D. Durand, J. D. Frankland, E. Galichet, E. Genouin-Duhamel, E. Gerlic, D. Guinet, P. Loutesse, J. L. Laville, J. F. Lecolley, R. Legrain, N. Le Neindre, O. Lopez, M. Louvel, A. M. Maskay, L. Nalpas, A. D. Nguyen, M. Parlog, J. Peter, M. F. Rivet, E. Rosato, F. Saint-Laurent, S. Salou, J. C. Steckmeyer, M. Stern, G. Tabacaru, B. Tamain, L. Tassan-Got, O. Tirel, E. Vient, C. Volant, J. P. Wieleczko (The INDRA Collaboration), *Phys. Rev. C* **61**, 014606 (1999).
- [79] M. Di Toro, A. Olmi, and R. Roy, *Eur. Phys. J. A* **30**, 65 (2006).
- [80] M. Mjahed, Ph.D. thesis, University of Clermont-Ferrand, 1987 (unpublished).
- [81] V. E. Viola, Jr., *Nucl. Data Sect. A* **1**, 391 (1966).
- [82] H. Lu, Ph.D. thesis, University of Caen, Caen, France, 2015 (unpublished).
- [83] C. Shen, G. Kosenko, and Y. Abe, *Phys. Rev. C* **66**, 061602 (2002).
- [84] C. Shen *et al.*, *Int. J. Mod. Phys. E* **17**, 66 (2008).
- [85] C. W. Shen, Y. Abe, Q. F. Li, and D. Boilley, *Sci. China Ser G* **52**, 1458 (2009); C. W. Shen, D. Boilley, Q. Li, J. Shen, and Y. Abe, *Phys. Rev. C* **83**, 054620 (2011).
- [86] R. Bougault *et al.*, *Eur. Phys. J. A* **50**, 47 (2014).
- [87] D. Lacroix, A. Van Lauwe, and D. Durand, *Phys. Rev. C* **69**, 054604 (2004); D. Lacroix and D. Durand, [arXiv:nucl-th/0505053](https://arxiv.org/abs/nucl-th/0505053) (unpublished); D. Lacroix, V. Blideanu, and D. Durand, *Phys. Rev. C* **71**, 024601 (2005).
- [88] R. Charity *et al.*, *Nucl. Phys. A* **476**, 516 (1988).
- [89] J. D. Frankland *et al.*, (unpublished).